Biophysical Journal, Volume 98

Supporting Material

Fluorescence spectral dynamics of single LHCII trimers

Tjaart P.J. Krüger, Vladimir I. Novoderezhkin, Cristian Ilioaia, and Rienk van Grondelle

Fluorescence spectral dynamics of single LHCII trimers

Tjaart P.J. Krüger, Vladimir I. Novoderezhkin, Cristian Ilioaia, and Rienk van Grondelle

This document comprises the following three sections:

1. Supplemental materials and methods, describing a gel-filtration chromatogram, the experimental setup, and calculation of spectral properties;
2. Calculation of the expected fluorescence, and the amount of energy absorption by the local environment;
3. Supplemental results, where some control experiments, comparison with the ensemble spectrum, and additional modeling results are described;
4. References

1. SUPPLEMENTAL MATERIALS AND METHODS

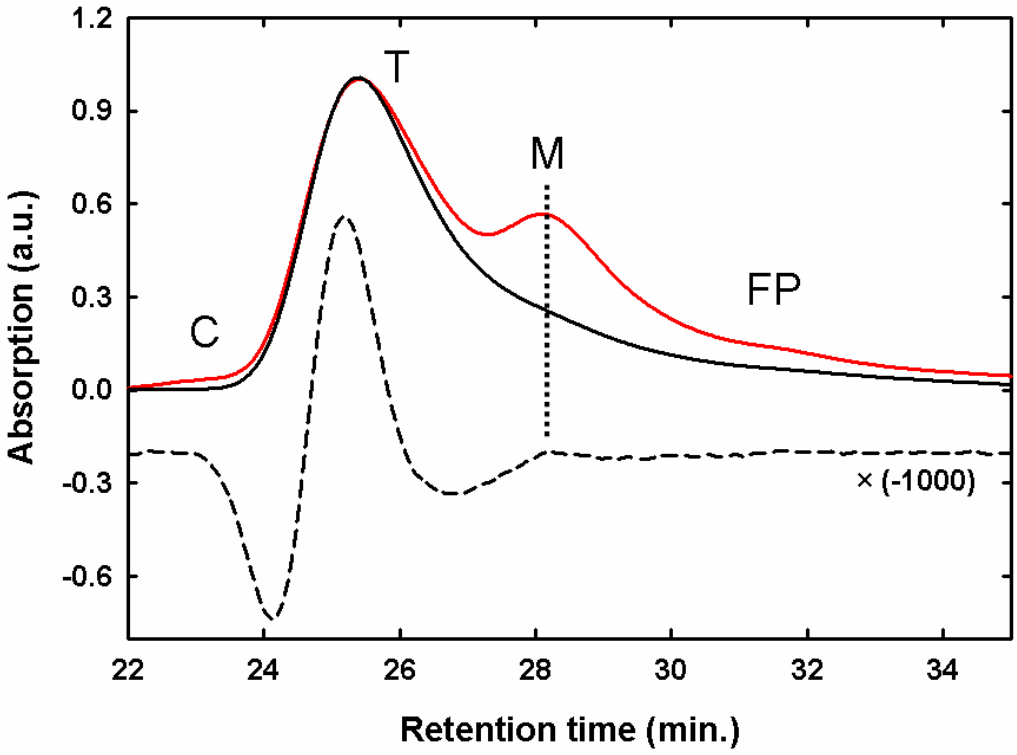

FIGURE S1 Gel-filtration chromatogram after first (*red*) and second (*black*) purifications, recorded at 630 nm, and inverted second derivative of second purification (*dashed*). The flow rate was 25 mL/h. The peaks at ~23.5 min, ~25.5 min, ~28 min and ~32 min correspond to contaminants (C), LHCII trimers (T), monomers (M) and free pigments (FP), respectively. The fraction collected after 25 min of the second purification was typically used.

Experimental setup

A commercial, inverted, wide-field microscope (Eclipse TE300; Nikon, Tokyo, Japan) was amended into a confocal microscope by adding a 100-μm diameter pinhole in the fluorescence beam path. A tunable, mode-locked Ti:Sapphire laser system (Mira 900, 76 MHz; Coherent, Santa Clara, CA), coupled to an optical parametric oscillator (Coherent) or BBO crystal (Casix, Fujian, China), enabled excitation in essentially the entire visible and near-UV region as well as into the NIR regime. Excitation pulses peaking at 630 nm were typically used. This allowed observation of large fluorescence spectral shifts to the blue and non-selective excitation of Chl *a* and *b*. The planar polarization of the light was changed into a near-circular state by a Berek polarization compensator (5540M; New Focus, Santa Clara, CA), and the beam was directed through a 100× magnification PlanFluor objective lens (1.3 NA, oil immersion, Nikon). The Berek compensator could at best achieve an elliptical eccentricity of ~0.87 (i.e., an

ellipticity of 2). In addition, the objective added ~10% to the ellipticity (equivalently ~3% to the eccentricity) of the polarization, supposedly caused by the CaF_2 coating of its lenses. The non-planar polarization ensured a minimized orientation dependence of the complexes. Operating the microscope in an epi-fluorescence configuration, the objective served to both focus the light tightly to a near-diffraction limit onto the complex-substrate interface and to efficiently collect the fluorescence from the same complex. In addition, a dichroic beam splitter (Z633RDC; Chroma Technology Corp., Rockingham, VT) served to separate the excitation and fluorescence beams with ~99% efficiency. The fraction of excitation light that was reflected and scattered by the coverslip and sample holder and traversing the dichroic was either blocked by the confocal pinhole holder or absorbed by a fluorescence filter (HQ645lp; Chroma Technology Corp.). The fluorescence light was focused either onto a point detector or dispersed onto a charge-coupled device (CCD) chip. These two highly sensitive detection devices were respectively a silicon avalanche photodiode (APD) single-photon counting module (SPCM-AQR-16; Perkin-Elmer Optoelectronics, Waltham, MA) and a liquid-nitrogen cooled, back-illuminated CCD camera (Spec10: 100BR; Princeton Instruments, Roper Scientific B.V., Vianen, The Netherlands). For efficient dispersion, either a loose grating (HR830/800nm; Optometrics LLC, Ayer, MA) or Shamrock 163i spectrograph (Andor Technology, Belfast, Northern Ireland), equipped with the grating SR1-GRT-0600-0750, was employed.

The sample was inserted into a home-designed, hermetically closed sample cell, equipped with a unit to stabilize the temperature at a fixed value between approximately –20°C and >100°C (1). A temperature of 5°C was typically used, which considerably prolonged the survival time of individual complexes upon continuous irradiation as compared to room-temperature conditions. Under these thermal and oxygen-free conditions, complexes in the dark remained stable for at least 1–2 days, as determined by their relative fluorescence intensity and survival time upon continuous irradiation. A typical excitation power of 0.9–1.0 μW (focal irradiance of 225–250 Wcm^{-2}) ensured an optimal signal-to-noise ratio (SNR), with relatively little photodamaging before irreversible photobleaching, as established by the stability of the emission properties or the reversibility of fluorescence fluctuations. At 630 nm, an excitation irradiance of ~240 Wcm^{-2} focused an average of ~4.5 photons per pulse on one complex, which yielded a detection rate of ~6000 and ~5000 counts per second (cps) by the APD and CCD camera, respectively. Under these conditions, a trimeric complex typically absorbed $(1.0 \pm 0.3) \times 10^8$ photons in 1–2 minutes before being photodamaged. The excitation intensity and ambient conditions remained constant during a measurement. A closed-loop two-dimensional piezo stage (P-713.8C; Physik Instrumente, Karlsruhe, Germany) controlled the position of the sample stage above the objective to subnanometer precision. Longitudinal drift of the focus was continually corrected by monitoring the reflected excitation light onto a monochrome video camera.

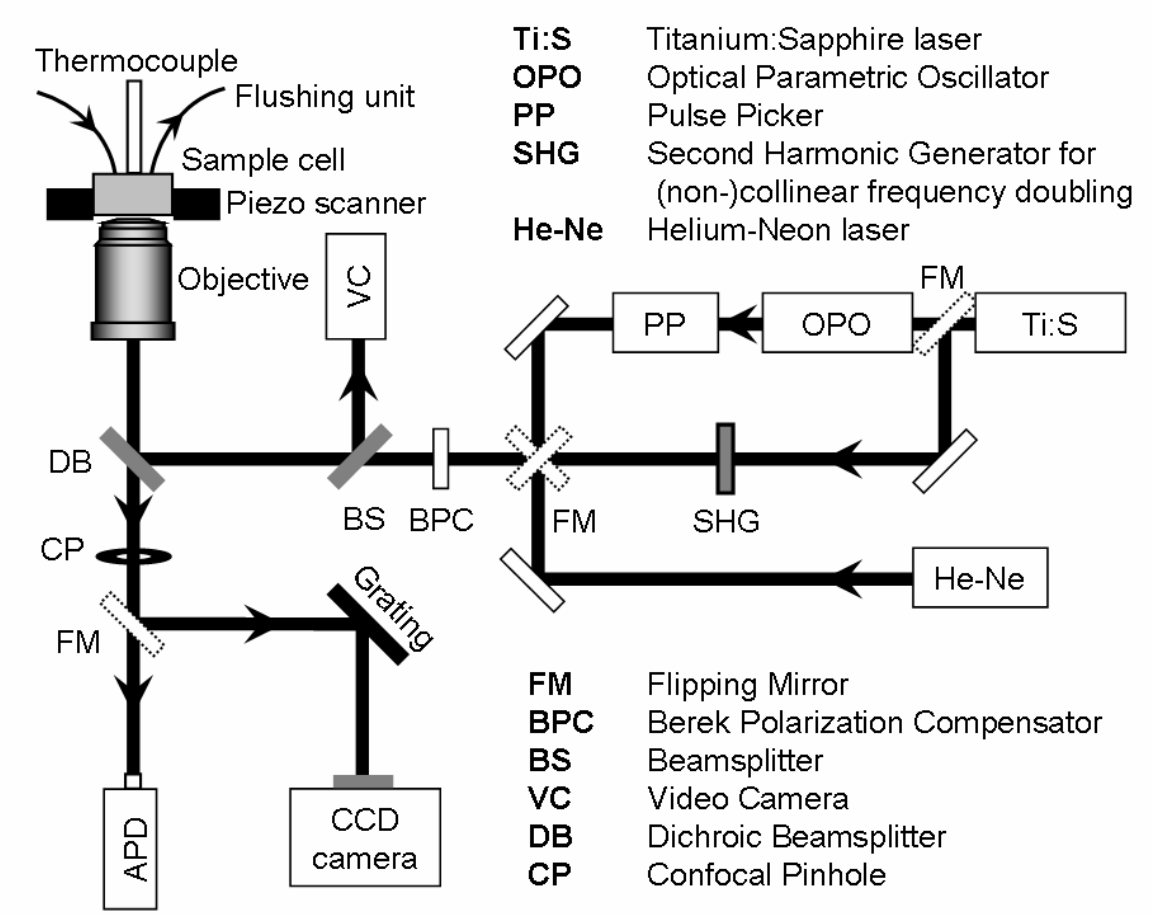

FIGURE S2 Simplified schematic of experimental setup, displaying its main optical components

Calculation of spectral properties

The fluorescence spectral profiles are reminiscent of a Gaussian shape with an enhanced wing and tail, typically to the red, and are accordingly well characterized by a skewed Gaussian function. Considering a skewness *b*, peak amplitude *A* and peak wavelength λ_m, the following function was typically used (2):

$$f(\lambda) = Ae^{-\frac{\ln 2}{b^2}\left[1+2b\frac{\lambda-\lambda_m}{\Delta\lambda}\right]^2},$$

where the width $\Delta\lambda$ is related to the full width at half maximum (FWHM) by $\mathrm{FWHM} = \Delta\lambda \sinh b/b$. An alternative function, which generally produced a slightly improved fit, describes the spectral values on one side of the maximum by a normal Gaussian function and on the other side with a skewed Gaussian:

$$f(\lambda)=\begin{cases} Ae^{-\frac{4\ln 2}{b^2}\left\{\ln[1+g(\lambda)(\lambda-\lambda_m)]\right\}^2} & \text{for } (\lambda-\lambda_m)b\le 0 \\ Ae^{-\frac{1}{2}\left(\frac{\lambda-\lambda_m}{\Delta\lambda}\right)^2} & \text{for } (\lambda-\lambda_m)b>0 \end{cases}$$

where

$$g(\lambda)=\frac{\sqrt{\ln 2}}{\Delta\lambda}\left(1-e^{-|b|}\right).$$

The FWHM is accordingly given by

$$\text{FWHM}=\frac{\Delta\lambda}{\sqrt{\ln 2}}e^{|b|/2}+2\Delta\lambda\sqrt{2\ln 2},$$

where the two terms stem from the skewed and normal Gaussian contributions, respectively.

The exact peak position was determined by fitting a simple Gaussian function within the FWHM window. A double skewed Gaussian function was used to fit double-band spectra where, particularly for the case of overlapping bands, the skewness and FWHM were restricted to correspond reasonably well with the values of single-band spectra. Fitting algorithms were based on the Nelmer-Mead or Levenberg-Marquardt algorithm in a least-mean-square optimization.

2. SUPPLEMENTAL CALCULATIONS

In this section, a number of calculations are performed to show that the measured complex is most likely a trimer. In addition, the temperature increase due to the absorbed radiation by the aqueous environment of the complex is calculated.

Expected fluorescence from LHCII trimers

The fluorescence flux emanating from a fluorescent system is related to the incident radiant flux Φ_I (also called the radiant power) as follows:

$$\Phi_f = \Phi_I \ \sigma_{10}\varphi_f \left(1-\eta_q\right), \tag{1}$$

where σ_{10} represents the effective ground state absorption cross-section, φ_f the fluorescence quantum yield, and η_q the quenching efficiency which denotes the probability that the excitation is lost due to multiphoton quenching processes. Note that intensity-independent quenching processes are included in the value of φ_f, whereas η_q describes intensity-dependent quenching. Defining the optical collection efficiency η_c, the number of detected fluorescence photons can be calculated by expressing Eq. 1 in terms of photon flux (counts per seconds):

$$N_f = \frac{I}{h\nu}\sigma_{10}\varphi_f\eta_c\left(1-\eta_q\right), \tag{2}$$

where I refers to the incident irradiation (often called “intensity”) and $h\nu$ the energy of a photon. Each parameter in Eq. 2 will be considered separately for an LHCII trimer.

(a) The photon flux density ($I / h\nu$) is approximated by considering a spatially Gaussian beam profile with an infinitely narrow spectral width. Consider such a beam propagating into the z direction and focused unto an LHCII trimer, with the trimer located in the center of the focus at $z = 0$. Let the beam waist (i.e., the focal beam radius) be defined by w_0. The radial intensity distribution at $z = 0$ is given by

$$I(r) = \frac{2P_0}{\pi w_0^2} e^{-2r^2/w_0^2}, \tag{3}$$

where P_0 is the total incident power, and r is the radial distance measured from z. It can readily be shown that the peak intensity I_0 relates to the beam power as $I_0 = 2P_0/\pi w_0^2$ (i.e., twice the average intensity within w_0) and the power through an aperture of radius r and centered at $z = 0$ is given by $P(r) = P_0\left(1-e^{-2r^2/w_0^2}\right)$.

Considering that an immobilized LHCII trimer is most likely oriented such that the incident beam is approximately perpendicular to the plane of the trimer, we can approximate the cross-sectional area of an LHCII trimer by the surface area of a circle with diameter 7.3 nm (3), i.e., r = 3.65 nm. The beam waist is determined by means of a raster scan, considering that the much smaller complex can be regarded as a point source, so that scanning across a complex is essentially a measure of the excitation point spread function (PSF). The diameter of the first lobe of the PSF, known as the Airy disk for a diffraction-limited focus, corresponds to the spot diameter and was measured to be ~1 μm, i.e., w_0 ~ 500 nm. (The discrepancy with the theoretical focal radius of $1.22\lambda / \mathrm{NA}$ for an excitation wavelength λ may be ascribed to the paraxial approximation in combination with chromatic aberration that results from the excitation and fluorescence wavelength difference in the high numerical-aperture objective.) A 630-nm beam that focuses 0.95 μW onto a trimer corresponds to an excitation intensity of 240 W cm^{-2} averaged over the area of a trimer (peak intensity 242 W cm^{-2}) and a photon flux density of 7.7×10^{20} s^{-1} cm^{-2}. This is equivalent to a photon flux of 3.2×10^{8} s^{-1} complex^{-1} or 4.5 photons pulse^{-1} at a pulse repetition rate of 76 MHz. [The corresponding photon density of ~10^{13} photons cm^{-2} pulse^{-1} is equivalent to typical pulse densities used in ensemble measurements (4, 5).]

(b) The absorption cross-section of LHCII σ_{10} was determined by means of two distinct semi-empirical methods, viz. (i) from the Chl *a* and *b* absorption spectra in an 80%-acetonic solution; and (ii) from the bulk trimeric LHCII absorption spectrum. The two methods give remarkably similar results. The effect of the polarization state of the incident light is first investigated.

The interaction Hamiltonian resulting from the electric dipole moment operator $\hat{\mathbf{d}}$ of the excited pigment and the positive frequency part of the electric field operator $\hat{\mathbf{E}}^{+}$ at the position of the pigment is given by $\hat{\mathbf{H}}_{\mathrm{int}} = -\hat{\mathbf{d}}(t) \cdot \hat{\mathbf{E}}^{+}(t)$. In the utilized steady state, the time dependence falls away. Defining φ and θ as the angles of the electric dipole vector relative to the propagation direction and the electric field vector, respectively, $\hat{\mathbf{H}}_{\mathrm{int}}$ is proportional to $\cos\theta \sin\varphi$ in the presence of planar polarized light. Since the electric field is always oriented perpendicularly to the propagation direction, different polarization modes of the incident light only affect the lateral component $f(\theta)$. For elliptically polarized light, the fraction of absorbed light in the lateral plane is proportional to the generic function

$$f(\theta) = \frac{1}{m}\left[1 + (m-1)\cos\theta\right], \tag{4}$$

where m is the ratio between the semimajor and -minor axes of the ellipse. Obviously, for circular polarization, $m = \infty$, and $\hat{\mathbf{H}}_{\text{int}}$ is a maximum. In our setup, we could at best achieve $m = 2$ with the Berek compensator. The objective adds an additional estimated 10% to the ellipticity, yielding m = 2.1. Accordingly, for a large set of randomly oriented pigments, an excitation efficiency of ~81% compared to circularly or randomly polarized light is achieved. Random values of φ add an additional reduction of ~36% (i.e., yielding ~64% of the maximum) for any type of excitation source. At 630 nm, primarily the Q_x-transition dipole moment of Chl *a* and the Q_y-transition dipole moment of Chl *b* are excited. Linear dichroism measurements have indicated that the distribution of these dipole moments of the pigments in LHCII can be considered random at this wavelength (6). Furthermore, empirical calculations of the absorption cross-section of the pigments in LHCII are generally based on the absorption efficiency of an ensemble of randomly oriented complexes irradiated by an incandescent lamp. The polarization dependence of such an excitation source is negligible (7). Calculations of the absorption efficiency of LHCII therefore need to consider only reduction due the absolute polarization of the incident light.

(i) We use the Chl *a* and *b* molar extinction coefficients given by ref. 8. At 630 nm, $\varepsilon_{\text{Chl } a} \approx \varepsilon_{\text{Chl } b} \approx 12$ $\text{mM}^{-1}\text{cm}^{-1}$. Considering a positive spectral shift of ~6.5 nm when projecting the values to a protein environment (9), and estimating an additional absolute absorption decrease of ~0.887 for this solvent replacement (11), the Chl *a* and *b* extinction coefficients at this wavelength in a protein environment are 11.2 and 9.7 $\text{mM}^{-1}\text{cm}^{-1}$, respectively. Including the decrease due to the utilized elliptically polarized light, the molar extinction coefficient of the full trimer at 630 nm is 358 $\text{mM}^{-1}\text{cm}^{-1}$, which is equivalent to an absorption cross-section of $\sigma_{10} = 1.37 \times 10^{-15}$ $\text{cm}^2 = 13.7$ Å^2.

(ii) For the bulk LHCII absorption, we employed the values given in ref. 2, *viz.*, total Chl concentration of 0.2 mg/mL, average Chl mass of 900 g/mol, beam pathlength of 1 mm, and OD of 0.44 at 645 nm. Considering OD(630 nm):OD(645 nm) ≈ 0.54, the average absorption cross-section of one Chl in the trimer in the presence of randomly-polarized light at 630 nm is 4.1×10^{-17} cm^2. Accordingly, the absorption cross-section of the full trimer irradiated with 630-nm elliptically-polarized light, is $\sigma_{10} = 1.39 \times 10^{-15}$ $\text{cm}^2 = 13.9$ Å^2.

(c) To estimate the fluorescence quantum yield φ_f, we propose that the significant dwell time of a complex in low-emission states may give rise to detection of short fluorescence lifetime components in ensemble measurements. We associate the longest lifetime components with the fully-emitting state, which is considered in this

calculation. Based on a number of literature values (10–16), we assume an average of 4 ns for the excited state lifetime τ_L of this state. Decay of this state is therefore proportional to e^{-t/τ_L}. The decay rate, defined by $k_L = \tau_L^{-1}$, is the sum of the radiative rate (k_r) and all nonradiative rates. The nonradiative processes can be classified into intersystem crossing (ISC), internal conversion (IC) and (residual) quenching, with decay rates denoted by k_{ISC}, k_{IC} and k_q, respectively. Thus,

$$k_L = k_r + k_{ISC} + k_{IC} + k_q . \tag{5}$$

The quantum yield related to each of these deexcitation channels, *i*, is defined by

$$\Phi_i = \frac{k_i}{k_L} . \tag{6}$$

In ref. 16, the value $k_r + k_{ISC} = (5.5\ \text{ns})^{-1}$ was estimated for a long excited-state lifetime component with an average lifetime of 4.5 ns. Assuming $k_q = 0$ for this component, from Eq. 5 follows $k_{IC} = 4 \times 10^7\ \text{s}^{-1}$. Note at this point that the fully-emitting state defined from the SMS measurements is in fact a time average of emissive properties on shorter timescales, i.e., short dwell times in low-emission states reduce the effective brightness of the excited system. For many systems, low-emission dwell times down to ~10-μs timescales have been observed (e.g., refs. 17–19), and even shorter dwell times may exist. Intensity time traces of trimeric LHCII show that this complex spends ~20% of its time in a low-emission state. We therefore estimate $\Phi_q \sim 0.2$. Assuming $k_L = (4\ \text{ns})^{-1}$, from Eq. 6 follows that $k_q = 5.0 \times 10^7\ \text{s}^{-1}$. Using these values for k_L and k_q, combined with the estimated value of k_{IC} calculated above and $k_{ISC} = 8.3 \times 10^7\ \text{s}^{-1}$ according to (20), Eq. 5 gives $k_r = 7.7 \times 10^7\ \text{s}^{-1}$. The corresponding fluorescence and triplet yield is 0.31 and 0.33, respectively. As expected, the triplet yield is substantially smaller than that of free chlorophyll (~0.64, ref. 21). In contrast, the fluorescence yield is similar to that of free chlorophylls in quenching-free conditions (22, 23). Furthermore, this value corresponds reasonably well with the value of 0.26 obtained by Duffy et al. (24) for trimeric LHCII, although it is still smaller than their overestimated model prediction of 0.38.

(d) A detection efficiency of ~8% of the full detection pathway into the APD was determined semi-empirically.

(e) The fluorescence saturation curve (Fig. S3) indicates that at least one source of intensity-dependent quenching exists for LHCII. We presume that excitation annihilation is the predominant source of saturation in high light. In particular, singlet-triplet (ST) annihilation is the dominant annihilation process in the relevant intensity window. The small photon absorption probability (~0.015 per pulse at 240

W cm^{-2}) clearly results in negligible single-singlet annihilation. However, using the triplet yield in (c), on average one triplet is formed every ~3 μs at 240 W cm^{-2}. Such a Chl triplet is rapidly quenched by a Car triplet (25), the latter which has a characteristic lifetime of 9–10 μs in oxygen-free solutions. Furthermore, since the inter-monomeric and inter-trimeric energy transfer timescales in LHCII are considerably shorter than the Car triplet decay time (26), the presence of one triplet in the excited system inevitably leads to ST annihilation upon absorption of all subsequent photons. Evidently, ST annihilation is the major quenching mechanism responsible for saturation in high light. To quantify this saturation, we notice that, on average, ~10 photons are absorbed before a Car triplet decays. Since a triplet is formed with a ~0.33 probability upon photon absorption, we can estimate that approximately two-thirds of the total number of absorbed photons are annihilated by ST annihilation, yielding a quenching efficiency η_q of ~0.67. [This value corresponds well with the expected fluorescence decrease when a mean number of z = 3 simultaneous excitations are used in a strongly coupled system where the total fluorescence yield scales as $(1-e^{-z})/z$ (27, 28). This function fits well to the experimental fluorescence saturation curve (Fig. S3).]

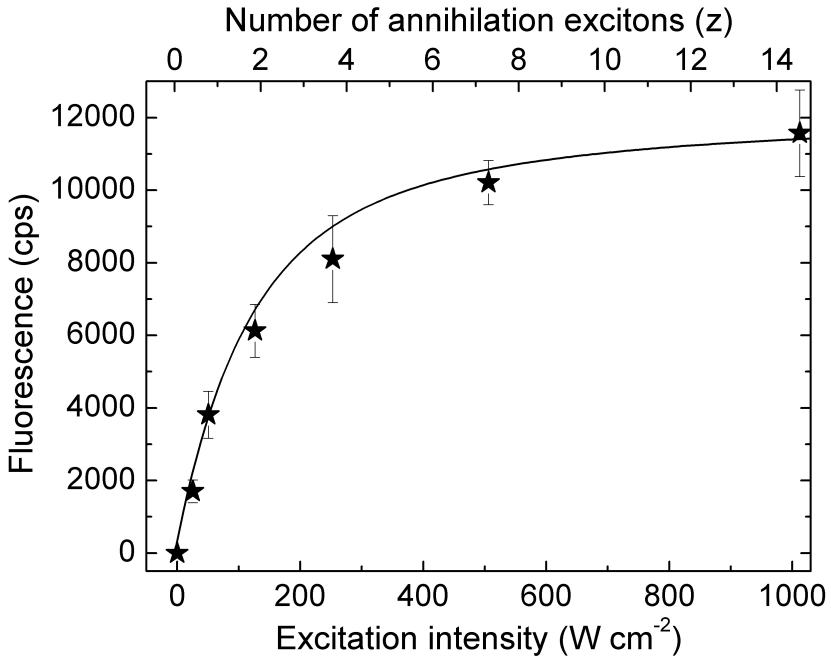

FIGURE S3 Saturation curve of the fluorescence (expressed in counts per second) as function of the excitation intensity and estimated number of annihilations, the latter which is predominantly responsible for saturation in high light. Error bars are the standard deviations of the calculated values. A fit of the function $(1-e^{-z})/z$ is shown (*solid line*).

From Eq. 2 it follows that the APD measures ~8700 cps when an LHCII trimer is irradiated with 240 W cm^{-2}. This value is consistent with the measured value of 7900 ± 1000 cps, confirming that the fluorescing unit is a trimer.

Energy absorption by the solvent

It was shown before that local heating in an LHCII trimer is negligible under the conditions employed in this experiment (29). This local heating was mainly attributed to exciton-exciton annihilation. It is simple to show that the solvent in the close vicinity of a trimer absorbs a negligible amount of laser energy.

Consider a focal volume defined by $r = z = 10$ nm in the center of the beam focus consisting of pure water molecules. In this volume we may assume a constant cross-sectional area and intensity of the beam. The power decrease of the incident light as the result of absorption along the length dz is then given by $dP(z) = I_0 A \alpha dz$, with α denoting the absorption coefficient of the medium, and the transverse cross-sectional area of the beam approximated by $A = \pi w_0^2$. Using α = 0.33 m^{-1} for water at 630 nm and 5°C (30), the total power absorbed in this focal region amounts to 6.6 × 10^{-15} W. Taking the specific heat capacity of water at 5°C to be 4.204 J K^{-1} mL^{-1}, the equivalent temperature increase is 2.6 nK per pulse, which is clearly negligible, considering that this heat is rapidly removed by the connected bath of 5°C.

3. SUPPLEMENTAL RESULTS

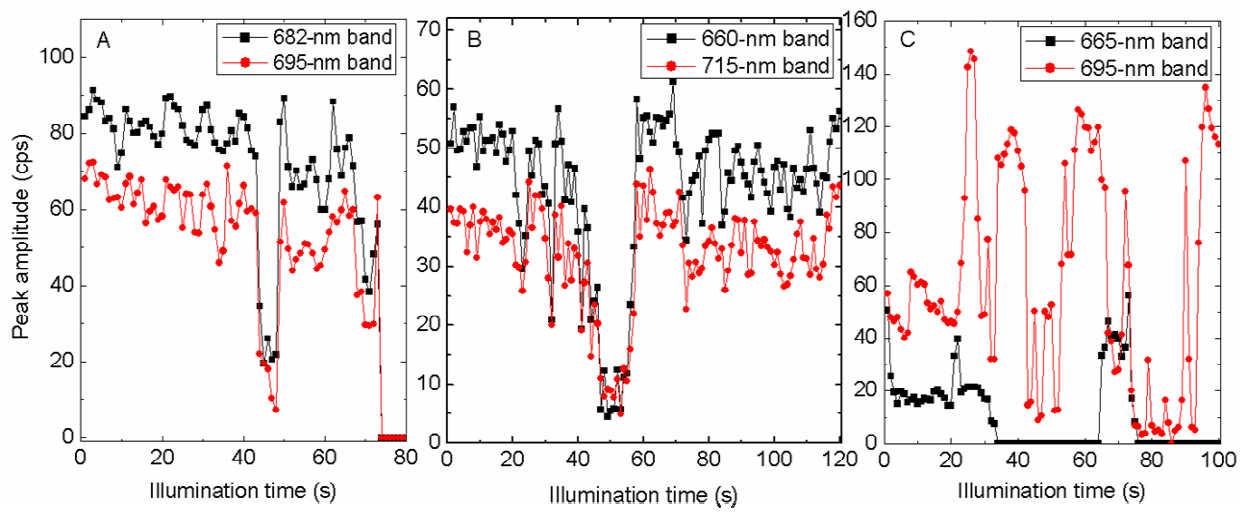

FIGURE S4 Examples of time-correlated (*A*, *B*) and -uncorrelated (*C*) fluctuations of double-band spectra. Correlated fluctuations occurred more frequently. Fluorescence was measured in counts per second (cps). The legends indicate the corresponding spectral peak values.

Control experiments

Apart from a number of controls mentioned in the main text, the effect of a different substrate and varying excitation rates was also investigated.

Replacement of the substrate with aminopropyltriethoxysilane (APTES) revealed no apparent difference in the spectral shape and peak wavelength distribution (data not shown). Although both substrates adhere to the complex predominantly electrostatically by means of their positively-charged terminal amino groups, the interaction with the complex is expected to be different for each substrate. This accordingly affects the mobility of the complex and the static disorder of the pigments to different extents. We conclude that the small difference in static disorder negligibly affects the total static disorder of the system.

The very low photon absorption probability per pulse (~0.015) resulted in a negligible contribution of singlet-singlet annihilation (see Supplemental Calculations). Accordingly, reduction of the repetition rate by means of a photoacoustic single pulse selector (APE GmbH) did not yield any noticeable improvements in the signal-to-noise ratio or in the photostability of the complex; on the contrary, maintaining the time-averaged fluorescence intensity demanded a higher excitation energy density per pulse, which resulted in increased levels of photodamage. However, a continuous-wave excitation source apparently slightly prolonged the survival time before photobleaching, whereas the fluorescence spectral activity was very similar to that of pulsed excitation.

Comparison with the ensemble spectrum

The steady-state ensemble spectrum of ~20,000 complexes compares well with the time and population average of a similar number of individually acquired spectra from single complexes (Fig. S5). The ensemble spectrum is slightly broader than the mean single-molecule spectrum. The discrepancy in the blue and red wings probably stems from slight differences in focusing onto the CCD chip from measurements performed on different days. The spectra of low-emitting states are included in the mean single-molecule spectrum, but elimination of these spectra did not notably affect the spectral shape. The similarity of the two spectral shapes indicates that the number of deviating states is independent of the excitation rate per complex and the illumination time; a larger access rate to deviating states is expected to broaden the single-molecule spectrum (1). A similar overlap between the bulk and mean single-molecule spectrum was found for other systems (31).

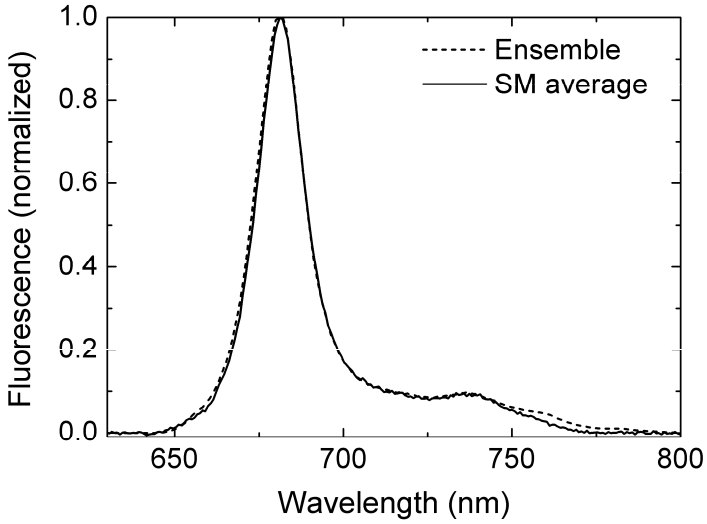

FIGURE S5 Bulk spectrum (*solid*) and time and population average of 400 complexes for ~60-second continuous illumination (*dashed*), measured under similar conditions. The ensemble spectrum was acquired upon 10-ms excitation of 0.1 μW, whereas 1-second excitation of 1 μW was used for every single-molecule (SM) spectrum.

Additional modeling results

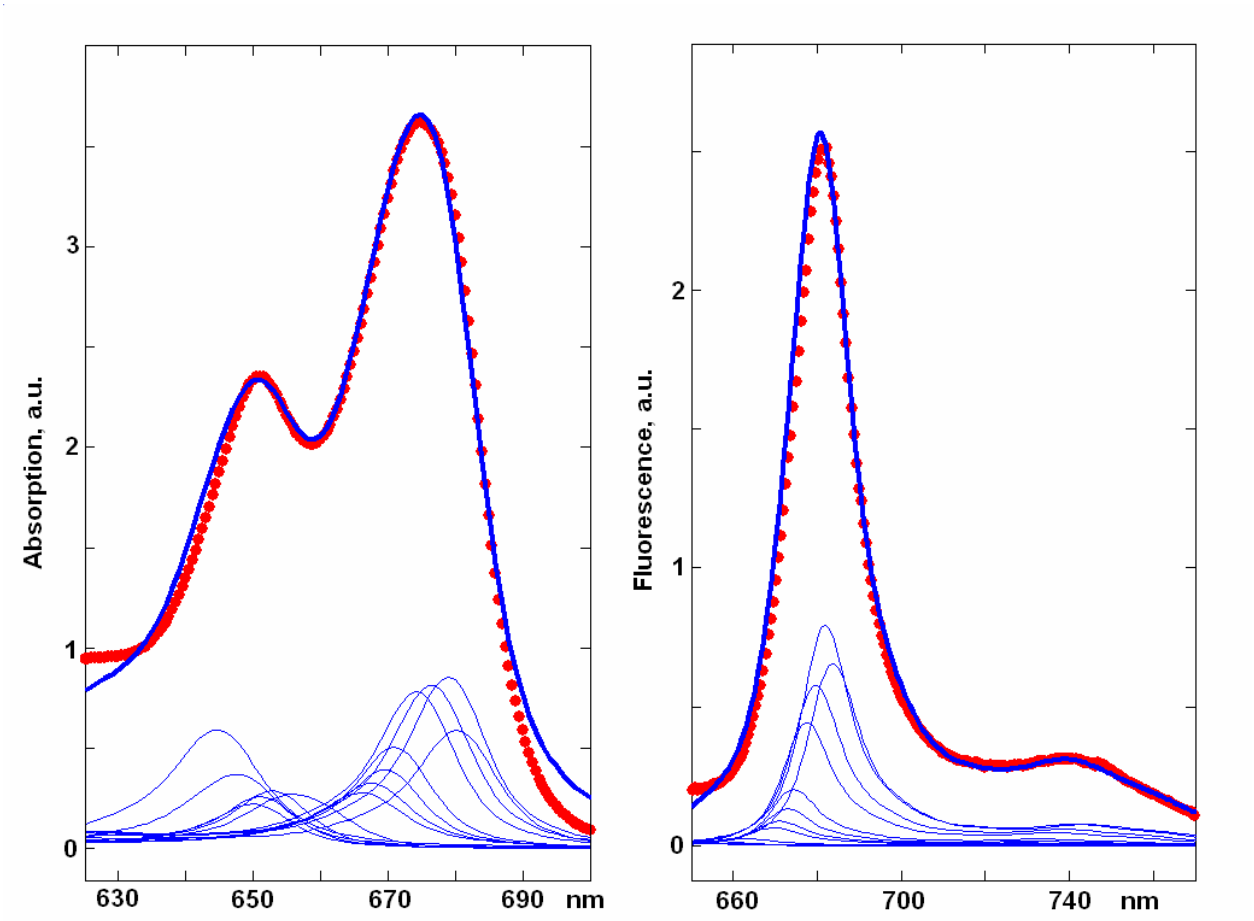

FIGURE S6 Steady-state bulk absorption and fluorescence spectra measured for trimeric LHCII at room temperature (*points*) and calculated using modified Redfield theory (*thick lines*). In the calculation we used the structural data of ref. 32 and our original exciton model of LHCII (33). Calculated spectra are shown together with contributions from the 14 individual exciton components (*thin lines*). See main text for more details.

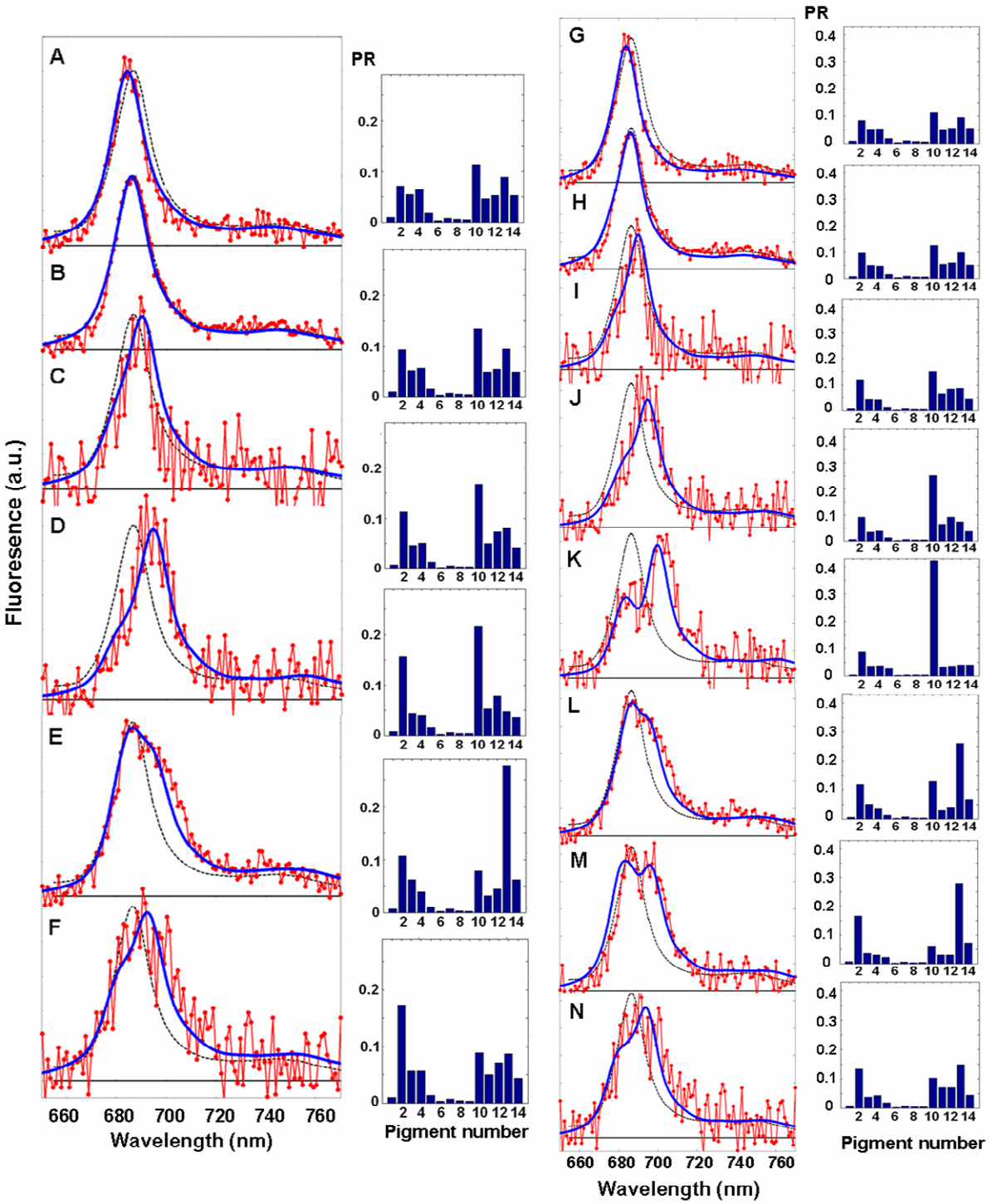

FIGURE S7 Comparison of selected modeled (*blue*) and measured (*red*) fluorescence spectral profiles, for normal static disorder (90 cm^{-1}) (*A–F*) and increased disorder (140 cm^{-1}) (*G–N*). Insets (blue histograms) denote the calculated thermally averaged participation ratio (PR) of the different pigments to the lowest exciton state. The equilibrium reference spectrum is depicted in black (*short, dashed line*) and all spectra are normalized. Measured spectra are averages of spectral profiles with similar shapes, and calculated spectra are averaged over a number of realizations.

From the 2000 calculated realizations in *A*–*F*, 26 spectra had an enhanced width, comprising 10 with a peak position near the bulk maximum and 16 with a red-shifted peak. *E* and *F* are averages of these 10 and 16 realizations, respectively. No realizations with a distinct double-peak shape were found among these 2000 realizations. Calculated spectra in panels *A*–*D* were averaged over 328, 976, 464, and 12 realizations peaking within 683.5–684.5, 685–686.5, 689–692, and 693–697 nm, respectively. Note that the individual realizations in each group have essentially the same characteristic line shape as the averaged spectrum for this group, with only a minor deviation in the peak position and width. Delocalization degrees for the 6 groups of realizations are described by the inverse participation ratio $1/\sum_n \mathrm{PR}_n$, with values 1.6807, 1.6102, 1.5123, 1.4039, 1.3618, and 1.5006 for Panels *A*–*F*, respectively. The inverse participation ratio of the steady-state density matrix (defined as in ref. 34) corresponding to each spectrum is given by 1.4219, 1.3933, 1.3127, 1.2404, 1.0611, and 1.3279, respectively.

Increase of the disorder (*G*–*N*) gave rise to larger inhomogeneous broadening and the presence of a few double-band spectra. Delocalization degrees for the 8 groups of realizations are 1.6334, 1.5765, 1.4809, 1.3930, 1.2893, 1.3013, 1.3191, and 1.4481 for panels *G*–*N*, respectively, and the respective participation ratios of the steady-state density matrix are 1.3887, 1.3604, 1.2914, 1.1506, 0.7834, 1.1139, 1.0332, and 1.3058.

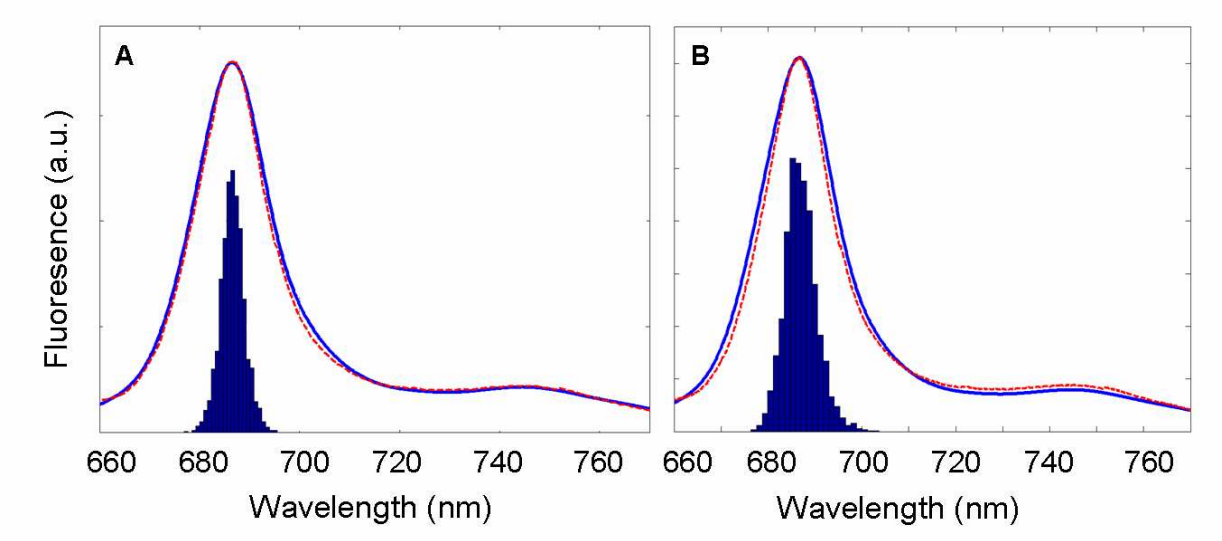

FIGURE S8 Distribution of fluorescence peak positions of 2000 calculated realizations of the static disorder, for disorder of 90 cm^{-1} (*A*) and 140 cm^{-1} (*B*). Calculated spectra averaged over the 2000 realizations are depicted in blue and compared with the time and population averaged measured spectrum (*red, dashed lines*).

Evidently, in our model the averaged spectrum is determined primarily by non-shifted realizations peaking at 682 ± 3 nm, with spectral shapes very similar to the bulk spectral profile. Spectral shapes with contributions shifted more than ~3 nm from the average position occur infrequently and therefore do not result in any significant broadening of the calculated averaged spectrum with respect to the bulk.

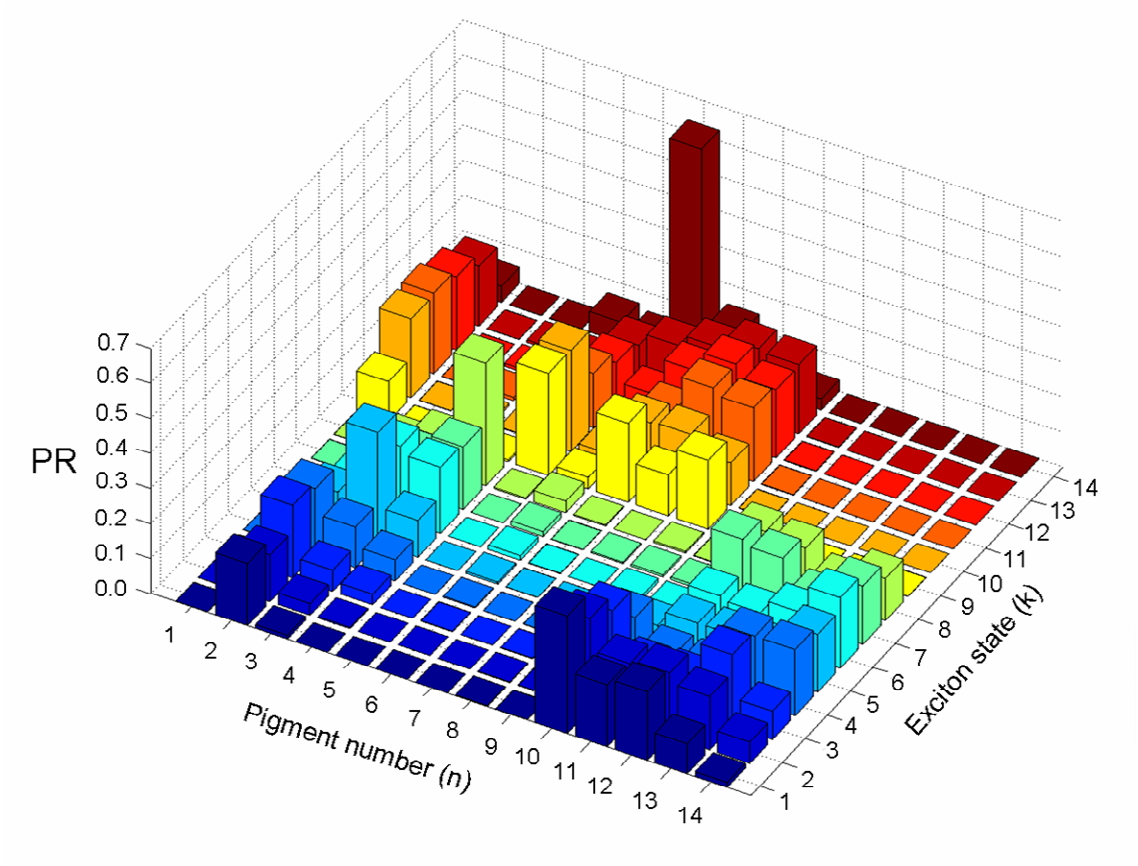

FIGURE S9 Participation ratio (PR) of the *n*-th pigment in the *k*-th exciton state, averaged over disorder. The lowest $k = 1$ state corresponds to excitation of the *a*610-*a*611-*a*612 cluster. Delocalization within this cluster is not uniform, but predominant localization is at *a*610. The delocalization within the other clusters can be explained similarly.

4. REFERENCES

1. Rutkauskas, D., V. I. Novoderezhkin, R. J. Cogdell, and R. van Grondelle. 2005. Fluorescence spectroscopy of conformational changes of single LH2 complexes. *Biophys. J.* 88:422–435.

2. Fraser, R. D. B., and Suzuki, E. 1969. Resolution of overapping bands: Functions for simulating band shapes. *Anal. Chem.* 41:37–39.

3. Kühlbrandt W., D. N. Wang, and Y. Fujiyoshi. 1994. Atomic model of plant light-harvesting complex by electron crystallography. *Nature.* 367:614–621.

4. Schödel, R. 1996. Kinetics of excited states of pigment clusters in solubilized light-harvesting complex II: Photon density-dependent fluorescence yield and transmittance. *Biophys. J.* 71:3370–3380.

5. Ruban A. V., R. Berera, C. Ilioaia, I. H. M. van Stokkum, J. T. M. Kennis, et al. 2007. Identification of a mechanism of photoprotective energy dissipation in higher plants. *Nature.* 450:575–U22.

6. Van Amerongen, H., S. L. S. Kwa, B. M. van Bolhuis, and R. van Grondelle. 1994 Polarized fluorescence and absorption of macroscopically aligned light harvesting complex II. *Biophys. J.* 67:837–847.

7. Kostuk, R. K. 1980. Polarization characteristics of DXW-type filament lamps. *App. Opt.* 19:2274–2275.

8. Cinque, G., R. Croce, and R. Bassi. 2000. Absorption spectra of chlorophyll a and b in Lhcb protein environment. *Photosynth. Res.* 64:233–242.

9. Zucchelli, G., D. Brogioli, A. P. Casazza, E. M. Garlaschi, and R. C. Jennings. 2007. Chlorophyll ring deformation modulates Q_y electronic energy in chlorophyll-protein complexes and generates spectral forms. *Biophys. J.* 93:2240–2254.

10. Croce, R., G. Cinque, A. R. Holzwarth, and R. Bassi. 2000. The Soret absorption properties of carotenoids and chlorophylls in antenna complexes of higher plants. *Photosynth. Res.* 64:221–231.

11. Moya, I., M. Silvestri, O. Vallon, G. Cinque, and R. Bassi. 2001. Time-resolved fluorescence analysis of the photosystem II antenna proteins in detergent micelles and liposomes. *Biochem.* 40:12552–12561.

12. Ide, J. P., D. R. Klug, W. Kühlbrandt, L. B. Giorgi, and G. Porter. 1987. The state of detergent solubilised light-harvesting chlorophyll-a/b protein complex as monitored by picosecond time-resolved fluorescence and circular dichroism. *Biochim. Biophys. Acta.* 893:349–364.

13. Vasil'ev, S., K.-D. Irrgang, T. Schrötter, A. Bergmann, H.-J. Eichler, and G. Renger. 1997. Quenching of chlorophyll *a* fluorescence in the aggregates of LHCII: Steady state fluorescence and picosecond relaxation kinetics. *Biochem.* 36:7503–7512.

14. Seydack, M., H. Redlin, and J. Voigt. 1995. On the dependence of LHC II fluorescence lifetimes on temperature. *In* Photosynthesis: From Light To Biosphere, Vol 1, P. Mathis, editor. Kluwer Academic Publishers, Dordrecht. 283–286.

15. Huyer, J., H.-J. Eckert, K.-D. Irrgang, J. Miao, H.-J. Eichler, and G. Renger. 2004. Fluorescence decay kinetics of solubilized pigment protein complexes from the distal, proximal, and core antenna of Photosystem II in the range of 10-277 K and absence or presence of sucrose. *J. Phys. Chem. B.* 108:3326–3334.

16. Palacios, M. A., J. Standfuss, M. Vengris, B. F. van Oort, I. H. M. van Stokkum, et al. 1996. A comparison of the three isoforms of the light-harvesting complex II using transient absorption and time-resolved fluorescence measurements. *Photosynth. Res.* 88:269–285.

17. Basché, T., S. Kummer, and C. Bräuchle. 1995. Direct spectroscopic observation of quantum jumps of a single molecule. *Nature.* 373:132–134.

18. Ha, T., T. Enderle, D. S. Chemla, P. R. Selvin, and S. Weiss. 1997. Quantum jumps of single molecules at room temperature. *Chem. Phys. Lett.* 271:1–5.

19. García-Parajó, M. F., G. M. J. Segers-Nolten, J. A. Veerman, J. Greve, and N. F. van Hulst. 2000. Real-time light-driven dynamics of the fluorescence emission in single green fluorescent protein molecules. *Proc. Natl. Acad. Sci. USA.* 97:7237–7242.

20. Kramer, H., and P. Mathis. 1980. Quantum yield and rate of formation of the carotenoid triplet state in photosynthetic structures. *Biochim. Biophys. Acta.* 593:319–329.

21. Seely, G. R., and J. S. Connolly. 1986. Fluorescence of photosynthetic pigments in vitro. *In* Light Emission by Plants and Bacteria. Govindjee, J. Amesz, and D. C. Fork, editors. Academic Press, New York. 99–133.

22. Latimer, P., T. T. Bannister, E. Rabinowitch. 1956. Quantum yields of fluorescence of plant pigments. *Science.* 124:585–586.

23. Weber, G., and F. W. J. Teale. 1957. Determination of the absolute quantum yield of fluorescent solutions. *Trans. Faraday Soc.* 53:646–655.

24. Duffy, C. D. P., A. V. Ruban, and W. Barford. 2008. Theoretical investigation of the role of strongly coupled chlorophyll dimers in photoprotection of LHCII. *J. Phys. Chem. B.* 112:12508–12515.

25. Peterman, E. J. G., F. M. Dukker, R. van Grondelle, and H. van Amerongen. 1995. Chlorophyll *a* and carotenoid triplet states in light-harvesting complex II of higher plants. *Biophys. J.* 69:2670–2678.

26. Van Grondelle, R., and V. I. Novoderezhkin. 2006. Energy transfer in photosynthesis: experimental insights and quantitative models. *Phys. Chem. Chem. Phy*s. 8:793–807.

27. Paillotin, G., C. E. Swenberg, J. Breton, and N. E. Geacintov. 1979. Analysis of picosecond laserinduced fluorescence phenomena in photosynthetic membranes utilizing a master equation approach. *Biophys. J.* 25:513–534.

28. Van Grondelle, R. 1985. Excitation energy transfer, trapping and annihilation in photosynthetic systems. *Biochim. Biophys. Acta.* 811: 147–195.

29. Gulbinas V., R. Karpicz, G. Garab, and L. Valkunas. 2006. Nonequilibrium heating in LHCII complexes monitored by ultrafast absorbance transients. *Biochem.* 45:9559–9565.

30. Sogandares, F. M., and E. S. Fry. 1997. Absorption spectrum (340–640 nm) of pure water. I. Photothermal measurements. *App. Opt.* 36:8699–8709.

31. Ying L., and X. S. Xie. 1998. Fluorescence spectroscopy, exciton dynamics, and photochemistry of single allophycocyanin trimers. *J. Phys. Chem. B.* 102:10399–10409.

32. Liu, Z. F., H. C. Yan, K. B. Wang, T. Y. Kuang, J. P. Zhang, et al. 2004. Crystal structure of spinach major light-harvesting complex at 2.72 Å resolution. *Nature*. 428:287–292.

33. Novoderezhkin, V. I., M. A. Palacios, H. van Amerongen, and R. Van Grondelle. 2005. Excitation dynamics in the LHCII complex of higher plants: Modeling based on the 2.72 Å crystal structure. *J. Phys. Chem. B.* 109:10493–10504.

34. Meier, T., V. Chernyak, and S. Mukamel. 1997. Femtosecond photon echoes in molecular aggregates *J. Chem. Phys.* 107:8759–8780.